iScience

CellPress
OPEN ACCESS

Article

Hsp70 exhibits a liquid-liquid phase separation ability and chaperones condensed FUS against amyloid aggregation

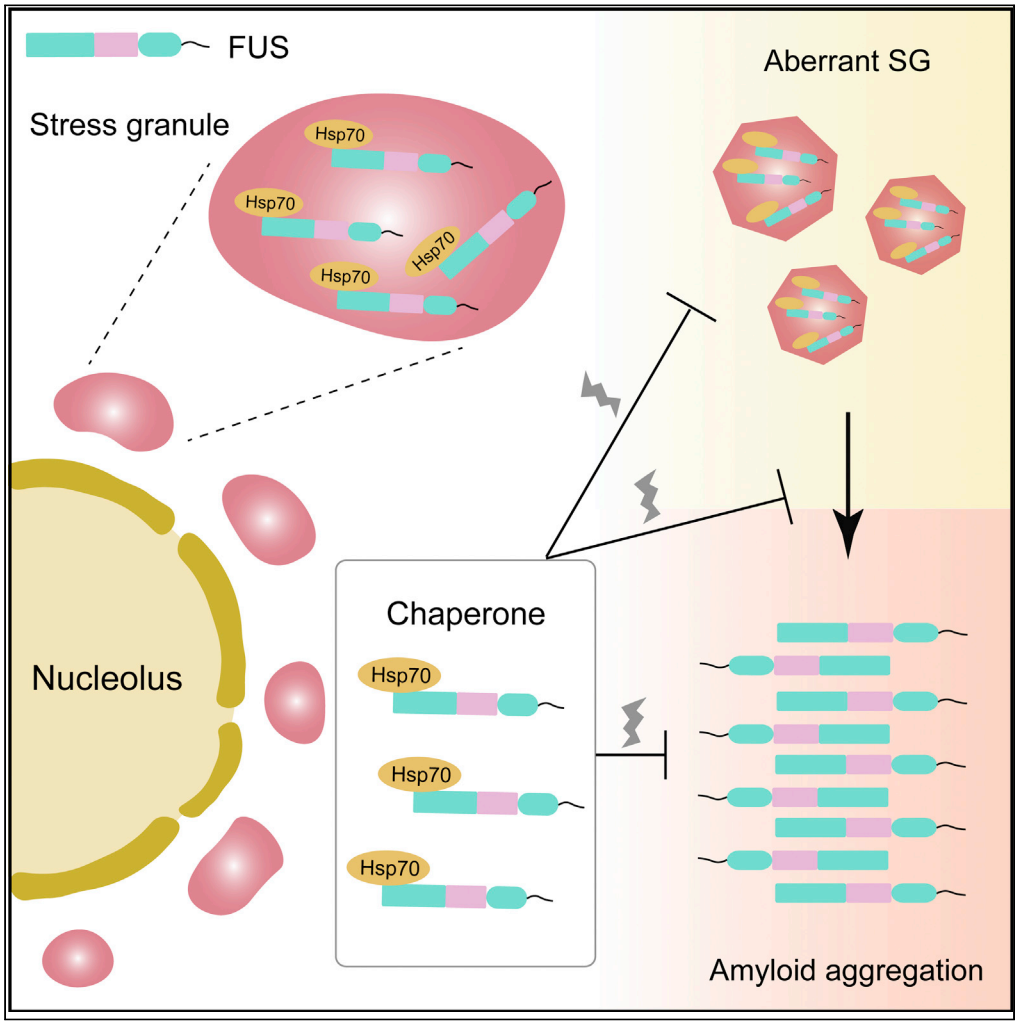

Yichen Li, Jinge Gu, Chen Wang, ..., Shengnan Zhang, Yanshan Fang, Dan Li

lidan2017@sjtu.edu.cn

Highlights

Hsp70 features a high ability of liquid-liquid phase separation *in vitro*

Hsp70 modifies liquid properties of SGs

Hsp70 inhibits the liquid-to-solid phase transition of FUS

Hsp70-CTD predominantly binds FUS-LC

Li et al., iScience *25*, 104356
June 17, 2022
https://doi.org/10.1016/j.isci.2022.104356

iScience

CellPress
OPEN ACCESS

Article

Hsp70 exhibits a liquid-liquid phase separation ability and chaperones condensed FUS against amyloid aggregation

Yichen Li,[1,2] Jinge Gu,[3,4] Chen Wang,[3,4] Jiaojiao Hu,[3,4] Shenqing Zhang,[1,2] Cong Liu,[3] Shengnan Zhang,[3] Yanshan Fang,[3] and Dan Li[1,2,5,6,*]

SUMMARY

Hsp70 is a key molecular chaperone in the protein quality control system to safeguard protein homeostasis in cells. Previous studies have shown that Hsp70 chaperones TDP-43, a pathogenic protein associated with amyotrophic lateral sclerosis (ALS), in nuclear bodies and prevents it from the pathological aggregation. In this work, we report that Hsp70 undergoes liquid-liquid phase separation, chaperones FUS, another ALS-linked pathogenic protein, in stress granules (SGs), and prevents condensed FUS from amyloid aggregation. Knock-down of Hsp70 does not influence SG assembly but results in the liquid-to-solid transition in SGs. NMR experiments further reveal Hsp70 predominantly uses its C-terminal substrate-binding domain to interact with the low complexity domain of FUS, which represents a mechanism distinct from that interacting with TDP-43. These findings suggest that Hsp70 is widely involved in chaperoning the physiological dynamics of various membrane-less organelles and adopts different mechanisms to prevent the pathological aggregation of different proteins.

INTRODUCTION

Molecular chaperones are key players in the protein quality control system, which are essential to maintain the protein homeostasis in cells (Hartl et al., 2011). A variety of chaperones widely exist in the cytoplasm and membrane-bound organelles such as nucleus, endoplasmic reticulum, and mitochondrion (Alderson et al., 2016; Moran Luengo et al., 2019). Recent studies have found that different chaperones such as Hsp90, Hsp70, and Hsp40 are also involved in the formation and regulation of different membrane-less organelles (MLOs) such as stress granules (SGs) and nuclear bodies (NBs) (Mateju et al., 2017; Jain et al., 2016; O'Meara et al., 2019; Gu et al., 2020; Yu et al., 2021; Gu et al., 2021; Pare et al., 2009; Frottin et al., 2019). For instance, it has been reported that Hsp70 is important to facilitate the generation and maintain the dynamics of the TDP-43 nuclear bodies (Yu et al., 2021; Gu et al., 2021). Hsp90 and AAA + ATPase VCP/p97 are involved in SG disassembly and degradation (Mediani et al., 2021; Wang et al., 2019). HspB8, Bag3, and Hsp70 form a chaperone network to maintain SG dynamics and integrity (Ganassi et al., 2016). These findings suggest that chaperones play an important role in regulating the protein homeostasis in different MLOs.

The dynamic assembly of MLOs is driven by protein liquid-liquid phase separation (LLPS) (Banani et al., 2017; Boeynaems et al., 2018; Boija et al., 2018; Brangwynne et al., 2009; Milovanovic et al., 2018; Strom et al., 2017; Su et al., 2016; Zeng et al., 2018). SG is one of the most intensively studied MLOs, in which SG-related proteins including G3BP, TIA1, and TDP-43 undergo LLPS to scaffold SG formation and further recruit protein and RNA components into SGs (Guillen-Boixet et al., 2020; Li et al., 2013; McGurk et al., 2018; Sanders et al., 2020; Yang et al., 2020). Under diseased conditions, the liquid-like nature of SGs is disrupted, which leads to aberrant SG solidification. Underlying this process, the amyloid-forming proteins in SGs including FUS, TDP-43, and hnRNPA1 may undergo liquid-to-solid phase transition to form amyloid aggregation, which is believed to be causative to neurodegenerative diseases such as amyotrophic lateral sclerosis (ALS) and frontotemporal dementia (FTD) (Fahrenkrog and Harel, 2018; Gasset-Rosa et al., 2019; Mackenzie et al., 2010; Molliex et al., 2015; Murakami et al., 2015; Patel et al., 2015; Ramaswami et al., 2013; Shukla and Parker, 2016). Hsp70 has been previously found to be recruited into SGs to assist SG disassembly (Ganassi et al., 2016; Jain et al., 2016). Hsp70 also exhibits a chaperone activity in preventing the pathological aggregation of TDP-43 in nuclear bodies (Gu et al.,

[1]Bio-X Institutes, Key Laboratory for the Genetics of Developmental and Neuropsychiatric Disorders, Ministry of Education, Shanghai Jiao Tong University, Shanghai 200030, China

[2]Zhangjiang Institute for Advanced Study, Shanghai Jiao Tong University, Shanghai 200240, China

[3]Interdisciplinary Research Center on Biology and Chemistry, Shanghai Institute of Organic Chemistry, Chinese Academy of Sciences, Shanghai 201210, China

[4]University of the Chinese Academy of Sciences, Beijing 100049, China

[5]Bio-X-Renji Hospital Research Center, Renji Hospital, School of Medicine, Shanghai Jiao Tong University, Shanghai 200240, China

[6]Lead contact

*Correspondence: lidan2017@sjtu.edu.cn

https://doi.org/10.1016/j.isci.2022.104356

2021). Importantly, Hsp70 level is downregulated in the spinal cord of patients with ALS (Chen et al., 2016), and increasing the Hsp70 level can rescue the neuropathology in ALS-related fly models (Coyne et al., 2017; Estes et al., 2011).

In this study, we found that Hsp70 directly interacts with FUS and chaperones the liquid-like state of SGs. Hsp70 exhibits a high ability of LLPS *in vitro*, and its co-phase separation with FUS prevents FUS from aberrant liquid-to-solid phase transition and fibrillation. The NMR study further reveals that Hsp70 uses its C-terminal substrate-binding domain (CTD) to bind the FUS low complexity (LC) domain. This mechanism is distinct from that underlying the interaction between Hsp70 and TDP-43. Our study reveals the essential role of Hsp70 in safeguarding SGs in the dynamic state and in preventing pathological protein aggregation.

RESULTS

Hsp70 undergoes LLPS and co-phase separates with FUS *in vitro* and in SGs

It has been shown in different experiments that Hsp70 and FUS are both components of SGs (Bosco et al., 2010; Jain et al., 2016; Markmiller et al., 2018; Mateju et al., 2017; Murray et al., 2017). To clarify whether these two proteins exist in the same spatiotemporal context, we immunostained Hsp70 and FUS, as well as G3BP1 (SG marker protein), simultaneously present in HeLa cells (Figure 1A). RFP-FUS R521H, an ALS-associated FUS mutant that tends to be involved in SGs (Guo et al., 2018), was overexpressed in the cells. The result showed that upon stress (100 μM sodium arsenite for 1 h), both endogenous Hsp70 and RFP-FUS R521H co-condenses into the G3BP1-positive SGs in HeLa cells (Figure 1A), and RFP failed to incorporate into SGs under stress conditions (Figure S1).

Given the co-condensation of Hsp70 and FUS in SGs, we next asked whether they have a direct interaction. FUS is well known to have a high ability of LLPS and can interact with several other proteins that are also able to undergo LLPS, such as hnRNPA1 and Hsp40 (Gu et al., 2020; Kamelgarn et al., 2016). We thus examined whether Hsp70 is able to undergo LLPS *in vitro*. We firstly purified recombinant Hsp70 fused with His-tag *in vitro*, and then cleaved His-tag to avoid its potential influence in Hsp70 LLPS (Figure S2). Next, we mapped the phase diagram of Hsp70 in the presence of molecular crowding agent PEG 3,350 and found that Hsp70 is able to spontaneously form liquid-like droplets with increasing concentration of protein and PEG 3,350 as revealed by differential interference contrast (DIC) and fluorescent images (Figure 1B). We confimed that PEG 3,350 is not involved in droplet formation (Figure S3). The fluorescence recovery after photobleaching (FRAP) assay showed that the fluorescence signal in the Hsp70 droplets rapidly recovered to ~70% in 500 s, indicating the liquid-like property of Hsp70 droplets (Figure 1C).

Hsp70 is composed of an N-terminal nucleotide-binding domain (NTD, residues 1–386) and a C-terminal substrate-binding domain (CTD, residues 387–641) (Figure S4A). To dissect the role of the two domains in mediating Hsp70 LLPS, we examined the LLPS ability of Hsp70-NTD and Hsp70-CTD, respectively. The result showed that both NTD and CTD are important for the LLPS ability of Hsp70, truncation of either domain resulted in a decreased LLPS ability (Figures S4B–S4D). Meanwhile, both domains exhibited LLPS capability (Figures S4B–S4D). FRAP analysis further confirmed the liquid-like property of the droplets formed by each individual domain (Figures S4E and SF).

Next, under the LLPS condition of Hsp70, we mixed sub-stoichiometric FUS-EGFP with Hsp70 (Hsp70:FUS = 25:1). DIC and fluorescence images showed that Hsp70 underwent LLPS. FUS-EGFP, which does not phase separate under this condition by its own, co-phase separated with Hsp70 (Figure 1D), suggesting the direct interaction between Hsp70 and FUS. Upon decreasing the concentration of Hsp70 below the threshold level, co-LLPS of Hsp70 and FUS-EGFP was eliminated (Figure S5A). In addition, we conversely mixed sub-stoichiometric Hsp70 with FUS-EGFP (FUS:Hsp70 = 10:1) under the LLPS condition of FUS and found co-LLPS of Hsp70 and FUS-EGFP (Figure 1E). The co-LLPS relied on the recruitment of Hsp70 by FUS-EGFP in the phase-separated state (Figure S5B). Meanwhile, to avoid the potential effect of EGFP on Hsp70 LLPS, we tested the co-LLPS of Hsp70 and EGFP. EGFP could not phase separate by its own (Figure S5D). Under the LLPS condition of Hsp70, EGFP did not co-phase separate with Hsp70 as shown by DIC and fluorescence imaging (Figure S5C). Taken together, these results showed that Hsp70 exhibits capability for LLPS *in vitro* and can co-phase separate with FUS both *in vitro* and in intracellular SGs.

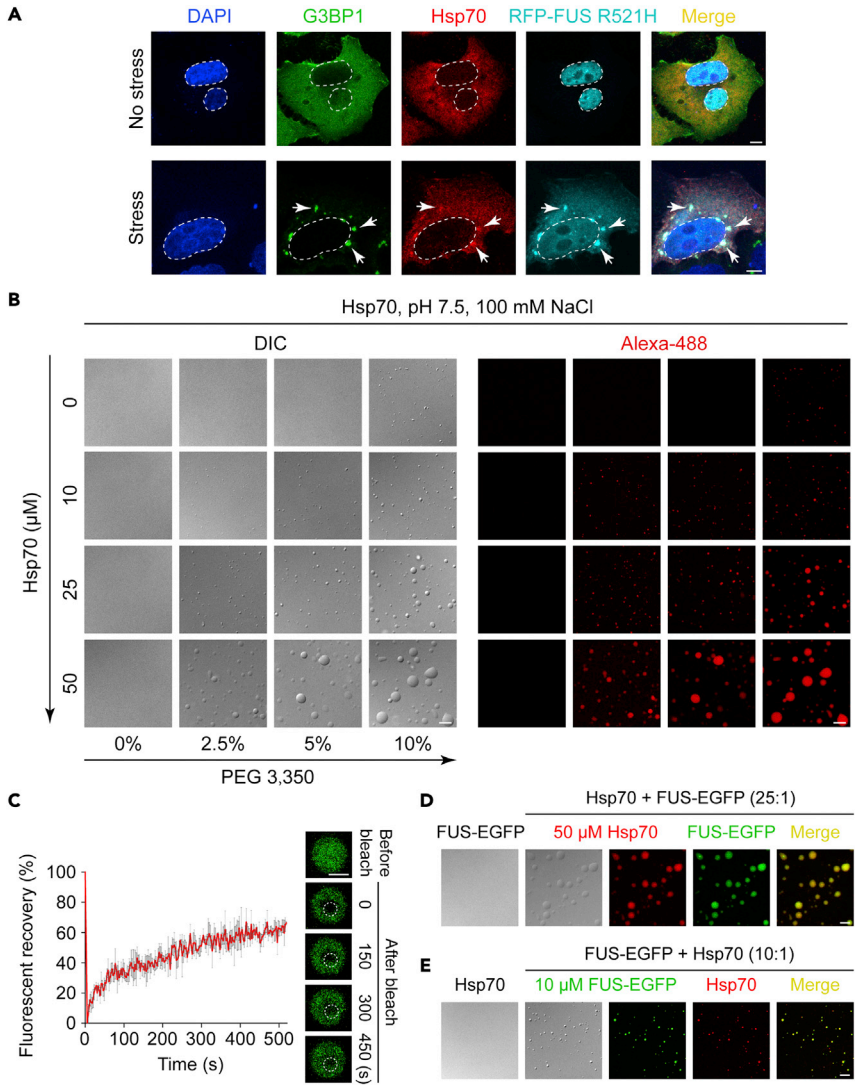

Figure 1. Hsp70 phase separates *in vitro* and colocalizes with FUS in SGs

(A) Confocal images of HeLa cells expressing RFP-FUS R521H. Cells were stressed with 100 μM sodium arsenite for 1 h and stained with antibodies for DAPI, Hsp70, and G3BP1. Scale bar, 5 μm. White arrows indicate SGs.

(B) DIC and fluorescence images of Hsp70 at indicated conditions. Buffer condition: 50 mM Tris-HCl (pH 7.5), 100 mM NaCl, PEG 3,350. Scale bar, 5 μm. (C) FRAP of Alexa 488 labeled Hsp70. FRAP curves and montages of a Hsp70 droplet are shown. Dashed circles indicate the bleached spot. Scale bar, 2 μm.

(D) DIC and fluorescence images show the incorporation of FUS-EGFP into Hsp70 droplets formed under the same condition as (B). The DIC image (left) indicates no LLPS of FUS-EGFP under this condition. Scale bar, 5 μm. The molar ratio of Hsp70 and FUS-EGFP is indicated.

(E) DIC and fluorescence images show the incorporation of Hsp70 into FUS-EGFP droplets. Buffer condition: 50 mM Tris-HCl (pH 7.5), 100 mM NaCl. The DIC image (left) indicates no LLPS of Hsp70 under this condition. Scale bar, 5 μm. See also Figures S1–S5.

Hsp70 chaperones the liquid-like state of SGs

We have previously shown that Hsp70 does not influence the assembly of SGs (Gu et al., 2021). To further investigate the influence of Hsp70 on the dynamics of SGs, we knocked down Hsp70 (encoded by *HSPA1A* and increased most dramatically in response to cellular stress) and Hsc70 (encoded by *HSPA8* and most abundant in HeLa cells) by transfection with small interference RNA (siRNA) of *HSPA1A* and *HSPA8* (si-Hsp70). Western blot analysis confirmed the reduced expression level of the total Hsp70 proteins by siRNAs (Figure S6). Consistent with our previous report (Gu et al., 2021), knockdown of Hsp70 showed

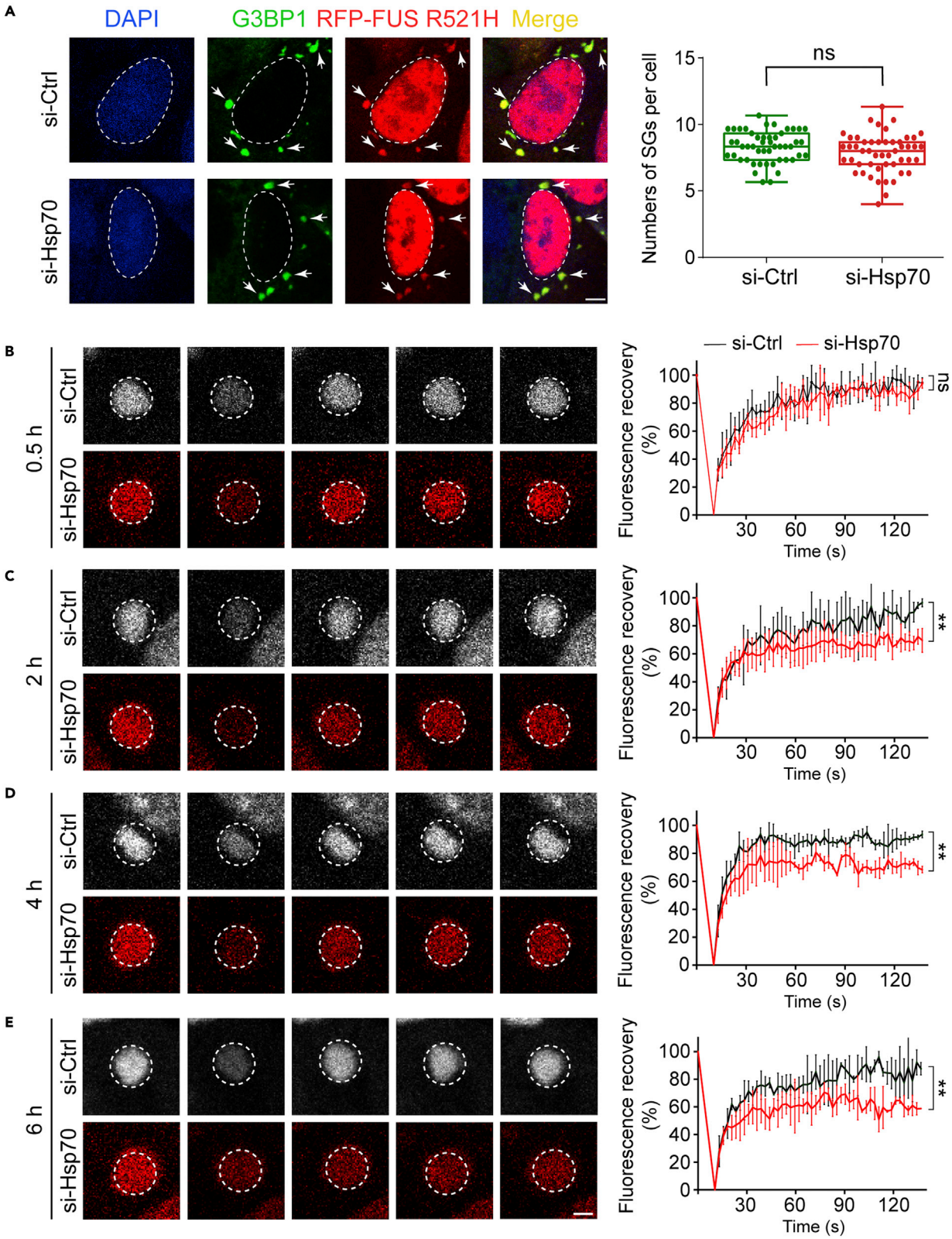
A
DAPI
G3BP1 RFP-FUS R521H
Merge
si-Ctrl
si-Hsp70
Numbers of SGs per cell
ns
si-Ctrl
si-Hsp70
B
0.5 h
si-Ctrl
si-Hsp70
si-Ctrl
si-Hsp70
Fluorescence recovery (%)
Time (s)
ns
C
2 h
**
D
4 h
**
E
6 h
**

Figure 2. Knockdown of Hsp70 promotes solidification of RFP-FUS R521H in SGs

(A) The effect of siRNAs (si-Ctrl/si-Hsp70) on the formation of SGs. Confocal images of HeLa cells expressing RFP-FUS R521H under arsenite stress are shown on the left. Cells were stained with antibodies for DAPI and G3BP1. White arrows indicate SGs. Scale bar, 5 μm. Quantification of numbers of SGs per cell in the imaging data is shown on the right. Values are means ± S.D., n > 150 cells from 3 replicates. Student's t test; ns, not significant.

(B–E) Fluorescence images of RFP-FUS R521H in SGs (left) and fluorescence recovery curves of the FRAP assay (right). HeLa cells transfected with negative control siRNA (si-Ctrl) or siRNAs against Hsp70 (si-Hsp70) are treated with arsenite for 0.5 h (b), 2 h (c), 4 h (d), or 6 h (e) as indicated. Dashed circles indicate the bleached spot. Data shown are means ± S.D., n = 3 individual SGs. Student's t test, ** $p < 0.01$; ns, not significant. Scale bar, 2 μm. See also Figures S6 and S7.

no significant influence on the numbers of FUS-R521H-positive SGs formed in cells (Figure 2A). However, *in situ* FRAP experiments showed that the Hsp70 knockdown significantly impaired the mobility of FUS-R521H within SGs over time (Figures 2B–2E). As the cells were stressed for 0.5 h, the fluorescence intensity of FUS-R521H recovered to nearly 100% within 135 s for both the control (si-Ctrl) and si-Hsp70 groups (Figure 2B). In contrast, as the duration of stress was gradually increased to 2–6 h, the signal recovery of FUS-R521H in the si-Hsp70 group was gradually impaired (Figures 2C–2E). After 6-h stress, only 60% of the fluorescence signals recovered within 135 s (Figure 2E), indicating solidification of FUS in SGs.

We next asked whether Hsp70 knockdown specifically impairs the internal dynamics of FUS or it also influences the internal mobility of other proteins in SGs. We examined the dynamics of G3BP1, the key scaffold protein of SGs, within SGs upon knocking down Hsp70 by *in situ* FRAP experiments. Importantly, we found that the internal mobility of G3BP1 is severely impaired in the si-Hsp70 groups but not the control group, especially in the cells stressed for 6 h (Figure S7). Taken together, our results showed that Hsp70 plays an essential role in maintaining not only the internal dynamics of FUS but also other proteins such as G3BP1 in SGs to safeguard the liquid-like state of SGs.

Hsp70 inhibits the liquid-to-solid phase transition of FUS into amyloid fibrils

We further examined the chaperone activity of Hsp70 in maintaining the dynamics of FUS in the liquid-like droplets *in vitro*. FUS-EGFP is able to readily form liquid-like droplets *in vitro* and exhibits superior internal mobility revealed by the FRAP assay (Figures 3A and 3B). Moreover, the liquid-like droplets of FUS-EGFP are able to spontaneously undergo the liquid-to-solid phase transition over time, and amyloid fibrils can be observed growing out of the droplets during the maturation process (Figure 3A). Although, Hsp70 forms liquid-like droplet without further solidification (Figure S8). Remarkably, co-phase separation of Hsp70 with FUS-EGFP maintained the liquid-like property of FUS-EGFP droplets and prevented FUS-EGFP from forming amyloid fibrils after 18-h incubation (Figures 3A and 3B).

Next, we assessed the activity of Hsp70 in preventing FUS amyloid fibrillation by combining the ThT kinetics assay and the negative-staining transmission electron microscopy (TEM). We overexpressed and purified FUS-LC, which is highly aggregation prone and was previously characterized to mediate FUS fibrillation. Indeed, FUS-LC spontaneously formed amyloid fibrils monitored by the ThT assay and TEM (Figures 3C and 3D). Notably, Hsp70 displayed a potent activity in inhibiting the amyloid fibrillation of FUS in a dose-dependent manner. The fibrillation of FUS is nearly completely suppressed in the presence of an equal molar of Hsp70 (Figures 3C and 3D). In addition, we confirmed that Hsp70 under the examined conditions does not form amyloid fibrils by its own (Figure S9). Taken together, our results show that Hsp70 exhibits a potent chaperone activity in maintaining the liquid-like property of FUS droplets and prevents condensed FUS from aberrant liquid-to-solid phase transition and fibrillation.

Hsp70-CTD predominantly binds FUS-LC

To further investigate the structural basis underlying the interaction between Hsp70 and FUS-LC, we performed the solution NMR spectroscopy. We firstly prepared ^{15}N-labeled FUS-LC and assigned its HSQC spectrum according to a previous study (Figures S10A and S10C) (Burke et al., 2015). Then, unlabeled Hsp70 was gradually titrated into the ^{15}N-labeled FUS-LC solution at pH 6.6. The result showed that the overall signal intensities of the residues of ^{15}N-labeled FUS-LC decreased gradually with the increasing concentrations of Hsp70 (Figure S11A), indicating the direct binding between FUS-LC and Hsp70. No obvious chemical shift was detected upon Hsp70 titration (Figure S10B). Intriguingly, the most dramatical intensity decrease (>55%) mainly occurred at serine residues of FUS-LC, as well as several other hydrophilic residues including Thr, Tyr, and Gln (Figure S11B), indicating hydrophilic interactions between Hsp70 and FUS-LC.

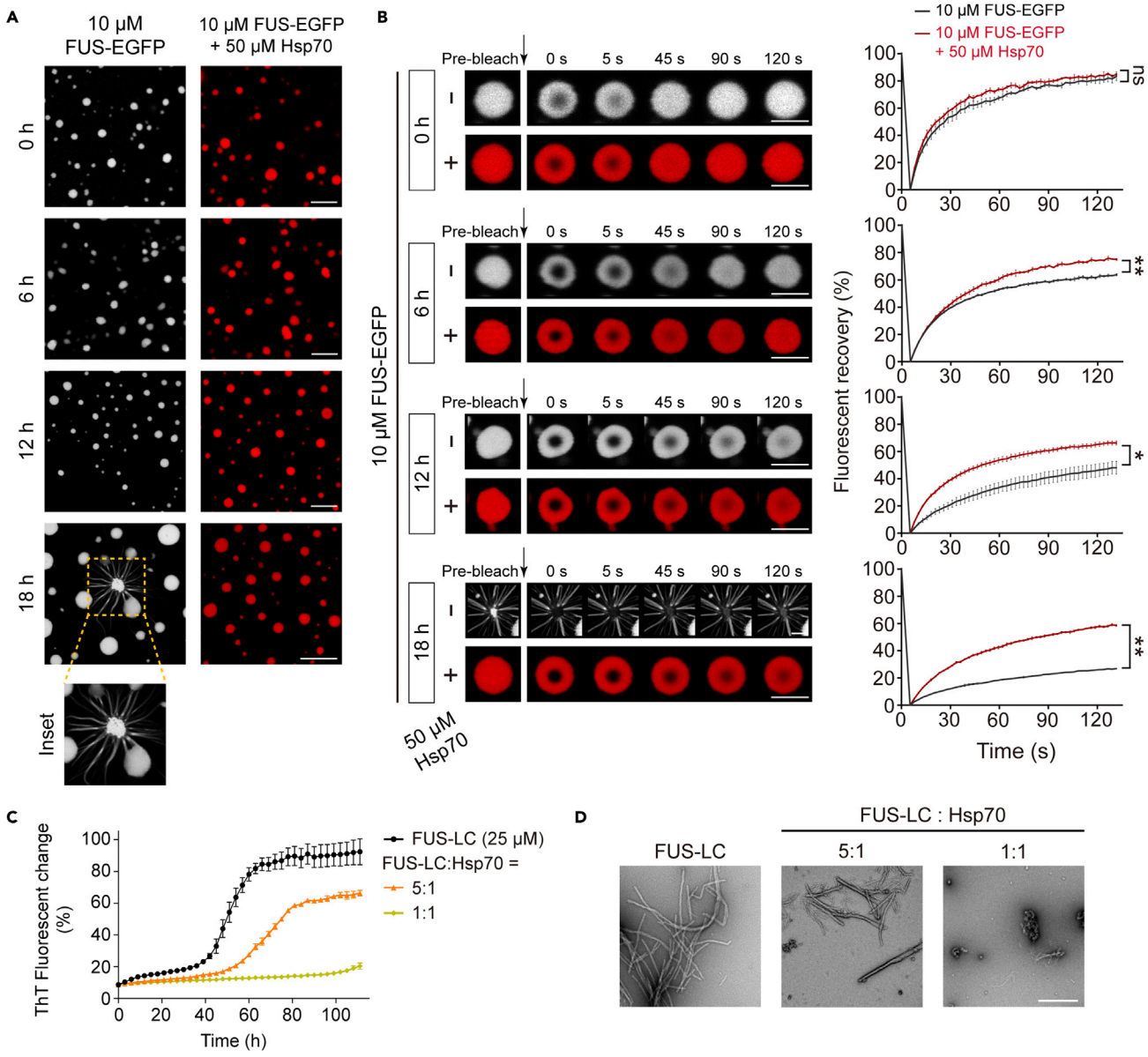

Figure 3. Hsp70 maintains FUS in the state of liquid-like droplets and prevents it from amyloid aggregation

(A) Representative images of the liquid-like droplets of FUS-EGFP in the absence or presence of Hsp70 in a maturation process of 18 h. Scale bar, 5 μm.

(B) FRAP images (left) and curves (right) of FUS-EGFP droplets in (a) are shown. Data are shown as mean ± SD with n = 3. Student's t test, * $p < 0.05$; ** $p < 0.01$; ns, not significant. Scale bar, 5 μm.

(C) The ThT fluorescence assay of FUS-LC (25 μM) with the addition of different concentrations of Hsp70. The molar ratios of FUS-LC to Hsp70 are indicated. Data correspond to mean ± SD, n = 3.

(D) Negative-staining TEM images of ThT samples at 110 h in (c). Scale bar: 500 nm. See also Figures S8 and S9.

To examine the effect of amide water exchange in the intensity change of Ser residue, we further performed the NMR experiments at pH 6.1, which may quench water exchange. The results showed that the number of residues with large intensity decrease (>55%) is largely decreased with no obvious preferential distribution for serine residues (Figures 4A and 4B). No obvious chemical shift deviations were detected upon Hsp70 titration at pH 6.1, which is similar to pH 6.6 (Figure S10D). Moreover, we predicted the water exchange rates for FUS-LC using SPHERE by Heinrich Roder at different pH and temperatures (Bai et al., 1993). The results show that the Ser residue has a higher water exchange efficiency compared with other amino acids at pH 6.6, and the water exchange value of Ser residue is significantly reduced by

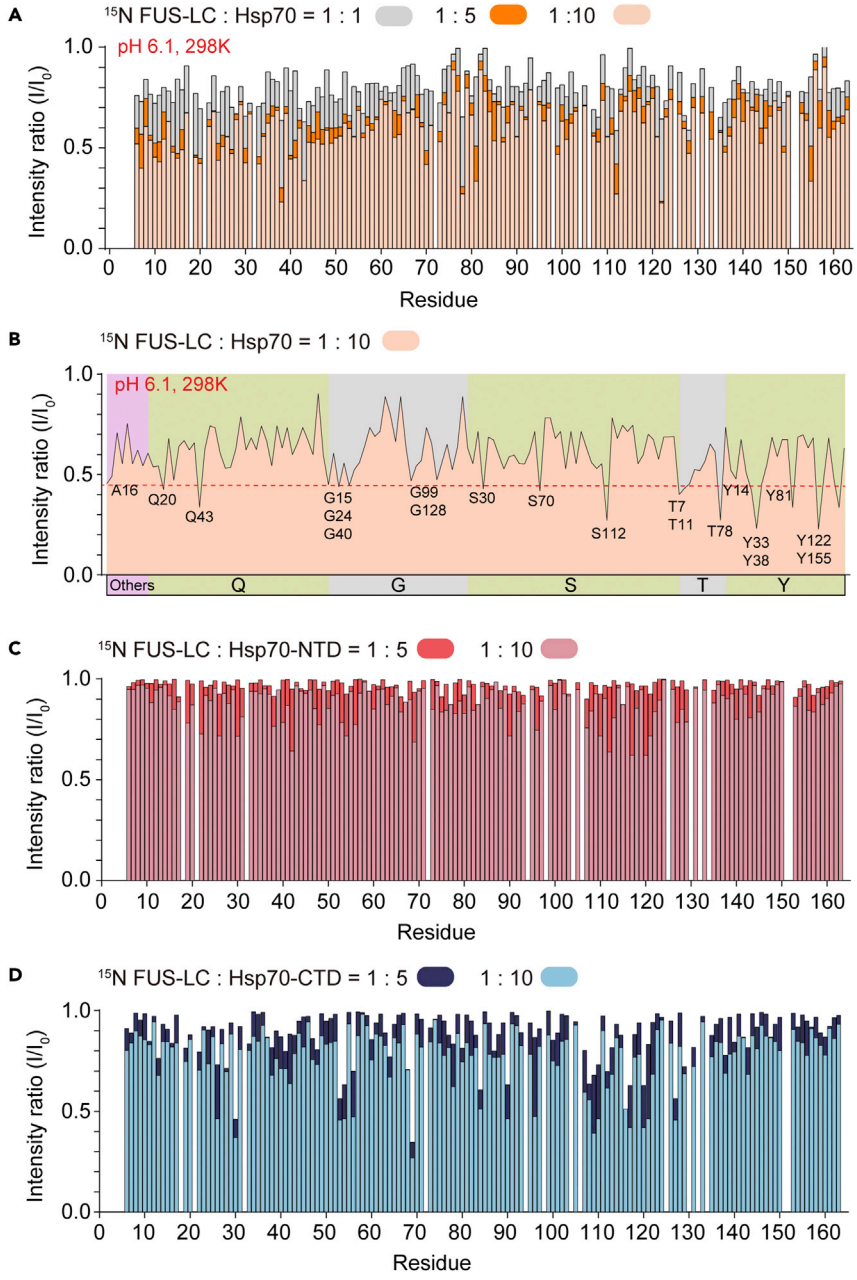

Figure 4. Residues intensity changes of signals in the 2D ^{1}H-^{15}N HSQC spectra of ^{15}N-labeled FUS-LC titrated by Hsp70

(A) Intensity changes of ^{15}N-labeled FUS-LC (25 μM) titrated by indicated molar ratios of Hsp70. Residues of FUS-LC are shown in consecutive numbers on the x axis.

(B) Intensity changes of ^{15}N-labeled FUS-LC (25 μM) titrated by Hsp70 (250 μM). Residues of FUS-LC are shown in groups on the x axis based on their types. The red dotted line indicates 45% signal intensities. Residues with intensity drops below 45% are marked.

(C and D) Intensity changes of ^{15}N-labeled FUS-LC (25 μM) titrated by indicated molar ratios of Hsp70-NTD (C) and Hsp70-CTD (D). See also Figures S10–S13.

lowering the temperature or pH. This may help to explain that the large signal decrease of Ser residues at pH 6.6 may at least partially come from water exchange (Figure S12). Together, our results show that Hsp70 directly binds to FUS-LC and induces the globally signal intensity reduction on multiple regions across the entire FUS-LC.

To further explore which domain of Hsp70 binds FUS-LC, we titrated ^{15}N-labeled FUS-LC with Hsp70-NTD and Hsp70-CTD, respectively. The result showed that although both domains induced the intensity drop of FUS-LC, Hsp70-CTD is apparently more potent than Hsp70-NTD (Figures 4C and 4D), and no obvious chemical shift was detected upon Hsp70 truncations titration (Figures S10E and S10F). In addition, consistent with the NMR results, Hsp70-CTD showed a higher activity in preventing FUS-LC fibrillation (Figure S13). Taken together, our results show that Hsp70 predominantly uses its CTD, which contains the substrate-binding domain, to bind with multiple regions cross FUS-LC to chaperone FUS-LC against amyloid aggregation.

DISCUSSION

Hsp70 has been found to be widely present in various MLOs such as TDP-43 nuclear bodies and SGs (Jain et al., 2016; Yu et al., 2021; Gu et al., 2021; Ganassi et al., 2016). Our work showed that Hsp70 exhibits a high ability of LLPS *in vitro*, which may drive the incorporation of Hsp70 into MLOs. The following important question is whether the LLPS capability of Hsp70 is essential in recruiting into MLOs and fulfilling its chaperone activity in different MLOs. Study on identification of the key residues for mediating Hsp70 LLPS will be important for further mutagenesis investigation to address this question.

Hsp70 is a key player in the protein quality control system and serves as a central node to bind other chaperones and co-chaperones (Kampinga and Craig, 2010). The condensation of Hsp70 in MLOs may further recruit its binding partners to form a chaperone network to co-operatively regulate the protein homeostasis in MLOs. The N-terminal nucleotide-binding domain (NTD) of Hsp70 is able to bind not only nucleotides but also other chaperones such as Hsp40 and Hsp110 and co-chaperones such as Bag1 (Jiang et al., 2007; Polier et al., 2008; Sondermann et al., 2001). Our previous findings showed that Hsp70-NTD predominantly binds a conserved region, which mediates the LLPS and amyloid aggregation, of TDP-43 (Gu et al., 2021). In sharp contrast, Hsp70 adopts a distinctive mechanism to bind FUS as we report in this work. The CTD, rather than NTD, predominantly binds to the FUS-LC. Previous studies identified several other chaperones, including Hsp27, TNPO1/kapβ2, and Hsp40, that can also bind to FUS and prevent its amyloid aggregation (Qamar et al., 2018; Liu et al., 2020; Gu et al., 2020; Yoshizawa et al., 2018; Guo et al., 2018; Hofweber et al., 2018). Interestingly, different chaperones employee distinct domains (e.g. N-terminal domain (NTD) and α-crystallin domain (ACD) of Hsp27 and G/F-rich region and C-terminal domain (CTD) of Hsp40, NTD, and CTD of Hsp70) to bind FUS-LC via different binding patterns (Figure S14). Thus, different chaperones may act solely or synergistically to safeguard FUS phase separation under different cellular circumstances.

In addition to molecular chaperones, RNA and other proteins in SGs were also found to regulate the assembly and dynamics of SGs, as well as modulate phase separation and aggregation of FUS, TDP-43, and other SG-containing proteins (Mann et al., 2019; Gwon et al., 2021). For instance, Donnelly et al found that RNA plays an important role in preventing TDP-43 from pathological aggregation (Mann et al., 2019). We found that the N protein from SARS-CoV-2 can enter SGs during virus infection, impairs the dynamic of SGs, and induces solidification of SGs. Moreover, the N protein directly binds with FUS and promotes its amyloid fibrils (Li et al., 2022), which is in sharp contrast to the effect of chaperones. Therefore, different types of proteins and RNA may exhibit different or even opposite effects in regulating phase separation of SG-containing protein as well as the assembly and dynamics of SGs.

FUS has been found to form amyloid aggregates in motor neurons of patients with ALS (Blair et al., 2010; Lai et al., 2011). Several mutations of FUS, such as G156E and R244C, have been identified in patients with familial ALS, which dramatically promote FUS amyloid aggregation (Patel et al., 2015). Thus, it will be interesting to further investigate how different regulators including chaperones and RNA cooperate to spatiotemporally regulate the physiological state of FUS and prevent it from pathological aggregation. Such studies may inform further efforts on the development of therapeutic treatment for ALS.

Limitations of the study

Hsp70 functions in cells in an ATP-dependent manner. Further studies are essential to explore whether ATP regulates the LLPS of Hsp70 and whether the LLPS of Hsp70 plays a role in cells.

STAR★METHODS

Detailed methods are provided in the online version of this paper and include the following:

- KEY RESOURCES TABLE

SUPPLEMENTAL INFORMATION

Supplemental information can be found online at https://doi.org/10.1016/j.isci.2022.104356.

ACKNOWLEDGMENTS

We thank staff members of the National Facility for Protein Science in Shanghai, Zhangjiang Laboratory, China for providing technical support and assistance in NMR data collection. This work was supported by the National Natural Science Foundation (NSF) of China (Grant No. 32170683, 82188101, 31872716 and 32171236), the Major State Basic Research Development Program (Grant No. 2019YFE0120600), the Science and Technology Commission of Shanghai Municipality (Grant No. 20XD1425000 and 2019SHZDZX02), CAS project for Young Scientists in Basic research (Grant No. YSBR-009), and the Shanghai Pilot Program for Basic Research – Chinese Academy of Science, Shanghai Branch (Grant No. CYJ-SHFY-2022-005).

AUTHOR CONTRIBUTIONS

Y.L. and D.L. designed the project. Y.L. and J.G. performed the *in vitro* characterization of protein phase separation and aggregation. Y.L., C.W., J.T., and S.Z. conducted the cellular experiments. Y.L. and S.Z performed the NMR experiments. All the authors are involved in analyzing the data and contributed to manuscript discussion and editing. Y.L. and D.L. wrote the manuscript.

DECLARATION OF INTERESTS

The authors declare no competing interests.

Received: October 13, 2021
Revised: March 5, 2022
Accepted: April 29, 2022
Published: June 17, 2022

REFERENCES

Alderson, T.R., Kim, J.H., and Markley, J.L. (2016). Dynamical structures of Hsp70 and hsp70-hsp40 complexes. Structure *24*, 1014–1030.

Bai, Y., Milne, J.S., Mayne, L., and Englander, S.W. (1993). Primary structure effects hydrogen exchange on peptide group. Proteins. *17*, 75–86.

Banani, S.F., Lee, H.O., Hyman, A.A., and Rosen, M.K. (2017). Biomolecular condensates: organizers of cellular biochemistry. Nat. Rev. Mol. Cell Biol. *18*, 285–298.

Blair, I.P., Williams, K.L., Warraich, S.T., Durnall, J.C., Thoeng, A.D., Manavis, J., Blumbergs, P.C., Vucic, S., Kiernan, M.C., and Nicholson, G.A. (2010). FUS mutations in amyotrophic lateral sclerosis: clinical, pathological, neurophysiological and genetic analysis. J. Neurol. Neurosurg. Psychiatry *81*, 639–645.

Boeynaems, S., Alberti, S., Fawzi, N.L., Mittag, T., Polymenidou, M., Rousseau, F., Schymkowitz, J., Shorter, J., Wolozin, B., Van Den Bosch, L., et al. (2018). Protein phase separation: a new phase in cell biology. Trends Cell Biol. *28*, 420–435.

Boija, A., Klein, I.A., Sabari, B.R., Dall'agnese, A., Coffey, E.L., Zamudio, A.V., Li, C.H., Shrinivas, K., Manteiga, J.C., Hannett, N.M., et al. (2018). Transcription factors activate Genes through the phase-separation capacity of their activation domains. Cell *175*, 1842–1855.e16.

Bosco, D.A., Lemay, N., Ko, H.K., Zhou, H., Burke, C., Kwiatkowski, T.J., Jr., Sapp, P., Mckenna-Yasek, D., Brown, R.H., Jr., and Hayward, L.J. (2010). Mutant FUS proteins that cause amyotrophic lateral sclerosis incorporate into stress granules. Hum. Mol. Genet. *19*, 4160–4175.

Brangwynne, C.P., Eckmann, C.R., Courson, D.S., Rybarska, A., Hoege, C., Gharakhani, J., Julicher, F., and Hyman, A.A. (2009). Germline P granules are liquid droplets that localize by controlled dissolution/condensation. Science *324*, 1729–1732.

Burke, K.A., Janke, A.M., Rhine, C.L., and Fawzi, N.L. (2015). Residue-by-Residue view of in vitro FUS granules that bind the C-terminal domain of RNA polymerase II. Mol. Cell *60*, 231–241.

Chen, H.J., Mitchell, J.C., Novoselov, S., Miller, J., Nishimura, A.L., Scotter, E.L., Vance, C.A., Cheetham, M.E., and Shaw, C.E. (2016). The heat shock response plays an important role in TDP-43 clearance: evidence for dysfunction in amyotrophic lateral sclerosis. Brain *139*, 1417–1432.

Coyne, A.N., Lorenzini, I., Chou, C.C., Torvund, M., Rogers, R.S., Starr, A., Zaepfel, B.L., Levy, J., Johannesmeyer, J., Schwartz, J.C., et al. (2017). Post-transcriptional inhibition of hsc70-4/HSPA8 expression leads to synaptic vesicle cycling defects in multiple models of ALS. Cell Rep. *21*, 110–125.

Delaglio, F., Grzesiek, S., Vuister, G.W., Zhu, G., Pfeifer, J., and Bax, A. (1995). NMRPipe: a multidimensional spectral processing system based on UNIX pipes. J. Biomol. NMR *6*, 277–293.

Estes, P.S., Boehringer, A., Zwick, R., Tang, J.E., Grigsby, B., and Zarnescu, D.C. (2011). Wild-type and A315T mutant TDP-43 exert differential neurotoxicity in a Drosophila model of ALS. Hum. Mol. Genet. *20*, 2308–2321.

Fahrenkrog, B., and Harel, A. (2018). Perturbations in traffic: aberrant nucleocytoplasmic transport at the heart of neurodegeneration. Cells *7*, 232.

Frottin, F., Schueder, F., Tiwary, S., Gupta, R., Korner, R., Schlichthaerle, T., Cox, J., Jungmann, R., Hartl, F.U., and Hipp, M.S. (2019). The nucleolus functions as a phase-separated protein quality control compartment. Science *365*, 342–347.

Ganassi, M., Mateju, D., Bigi, I., Mediani, L., Poser, I., Lee, H.O., Seguin, S.J., Morelli, F.F., Vinet, J., Leo, G., et al. (2016). A surveillance function of the HSPB8-BAG3-HSP70 chaperone complex ensures stress granule integrity and dynamism. Mol. Cell *63*, 796–810.

Gasset-Rosa, F., Lu, S., Yu, H., Chen, C., Melamed, Z., Guo, L., Shorter, J., Da Cruz, S., and Cleveland, D.W. (2019). Cytoplasmic TDP-43 de-mixing independent of stress granules drives inhibition of nuclear import, loss of nuclear TDP-43, and cell death. Neuron *102*, 339–357.e7.

Gu, J., Liu, Z., Zhang, S., Li, Y., Xia, W., Wang, C., Xiang, H., Liu, Z., Tan, L., Fang, Y., et al. (2020). Hsp40 proteins phase separate to chaperone the assembly and maintenance of membraneless organelles. Proc. Natl. Acad. Sci. U S A. *117*, 31123–31133.

Gu, J., Wang, C., Hu, R., Li, Y., Zhang, S., Sun, Y., Wang, Q., Li, D., Fang, Y., and Liu, C. (2021). Hsp70 chaperones TDP-43 in dynamic, liquid-like phase and prevents it from amyloid aggregation. Cell Res. *31*, 1024–1027.

Guillen-Boixet, J., Kopach, A., Holehouse, A.S., Wittmann, S., Jahnel, M., Schlussler, R., Kim, K., Trussina, I., Wang, J., Mateju, D., et al. (2020). RNA-induced conformational switching and clustering of G3BP drive stress granule assembly by condensation. Cell *181*, 346–361.e17.

Guo, L., Kim, H.J., Wang, H., Monaghan, J., Freyermuth, F., Sung, J.C., O'donovan, K., Fare, C.M., Diaz, Z., Singh, N., et al. (2018). Nuclear-import receptors reverse aberrant phase transitions of RNA-binding proteins with prion-like domains. Cell *173*, 677–692.e20.

Gwon, Y., Maxwell, B.A., Kolaitis, R.M., Zhang, P., Kim, H.J., and Taylor, J.P. (2021). Ubiquitination of G3BP1 mediates stress granule disassembly in a context-specific manner. Science *372*, eabf6548.

Hartl, F.U., Bracher, A., and Hayer-Hartl, M. (2011). Molecular chaperones in protein folding and proteostasis. Nature *475*, 324–332.

Hofweber, M., Hutten, S., Bourgeois, B., Spreitzer, E., Niedner-Boblenz, A., Schifferer, M., Ruepp, M.D., Simons, M., Niessing, D., Madl, T., and Dormann, D. (2018). Phase separation of FUS is suppressed by its nuclear import receptor and arginine methylation. Cell *173*, 706–719.e13.

Jain, S., Wheeler, J.R., Walters, R.W., Agrawal, A., Barsic, A., and Parker, R. (2016). ATPase-modulated stress granules contain a diverse proteome and substructure. Cell *164*, 487–498.

Jiang, J., Maes, E.G., Taylor, A.B., Wang, L., Hinck, A.P., Lafer, E.M., and Sousa, R. (2007). Structural basis of J cochaperone binding and regulation of Hsp70. Mol. Cell *28*, 422–433.

Kamelgarn, M., Chen, J., Kuang, L., Arenas, A., Zhai, J., Zhu, H., and Gal, J. (2016). Proteomic analysis of FUS interacting proteins provides insights into FUS function and its role in ALS. Biochim. Biophys. Acta *1862*, 2004–2014.

Kampinga, H.H., and Craig, E.A. (2010). The HSP70 chaperone machinery: J proteins as drivers of functional specificity. Nat. Rev. Mol. Cell Biol. *11*, 579–592.

Lai, S.L., Abramzon, Y., Schymick, J.C., Stephan, D.A., Dunckley, T., Dillman, A., Cookson, M., Calvo, A., Battistini, S., Giannini, F., et al. (2011). FUS mutations in sporadic amyotrophic lateral sclerosis. Neurobiol. Aging *32*, 550.e1–550.e4.

Lee, W., Tonelli, M., and Markley, J.L. (2015). NMRFAM-SPARKY: enhanced software for biomolecular NMR spectroscopy. Bioinformatics *31*, 1325–1327.

Li, Y.R., King, O.D., Shorter, J., and Gitler, A.D. (2013). Stress granules as crucibles of ALS pathogenesis. J. Cell Biol. *201*, 361–372.

Li, Y., Lu, S., Gu, J., Xia, W., Zhang, S., Zhang, S., Wang, Y., Zhang, C., Sun, Y., Lei, J., et al. (2022). SARS-CoV-2 impairs the disassembly of stress granules and promotes ALS-associated amyloid aggregation. Protein Cell *7*, 232.

Liu, Z., Zhang, S., Gu, J., Tong, Y., Li, Y., Gui, X., Long, H., Wang, C., Zhao, C., Lu, J., et al. (2020). Hsp27 chaperones FUS phase separation under the modulation of stress-induced phosphorylation. Nat. Struct. Mol. Biol. *27*, 363–372.

Mackenzie, I.R., Rademakers, R., and Neumann, M. (2010). TDP-43 and FUS in amyotrophic lateral sclerosis and frontotemporal dementia. Lancet Neurol. *9*, 995–1007.

Mann, J.R., Gleixner, A.M., Mauna, J.C., Gomes, E., Dechellis-Marks, M.R., Needham, P.G., Copley, K.E., Hurtle, B., Portz, B., Pyles, N.J., et al. (2019). RNA binding antagonizes neurotoxic phase transitions of TDP-43. Neuron *102*, 321–338.e8.

Markmiller, S., Soltanieh, S., Server, K.L., Mak, R., Jin, W., Fang, M.Y., Luo, E.C., Krach, F., Yang, D., Sen, A., et al. (2018). Context-dependent and disease-specific diversity in protein interactions within stress granules. Cell *172*, 590–604.e13.

Mateju, D., Franzmann, T.M., Patel, A., Kopach, A., Boczek, E.E., Maharana, S., Lee, H.O., Carra, S., Hyman, A.A., and Alberti, S. (2017). An aberrant phase transition of stress granules triggered by misfolded protein and prevented by chaperone function. EMBO J. *36*, 1669–1687.

McGurk, L., Gomes, E., Guo, L., Mojsilovic-Petrovic, J., Tran, V., Kalb, R.G., Shorter, J., and Bonini, N.M. (2018). Poly(ADP-Ribose) prevents pathological phase separation of TDP-43 by promoting liquid demixing and stress granule localization. Mol. Cell *71*, 703–717.e9.

Mediani, L., Antoniani, F., Galli, V., Vinet, J., Carra, A.D., Bigi, I., Tripathy, V., Tiago, T., Cimino, M., Leo, G., et al. (2021). Hsp90-mediated regulation of DYRK3 couples stress granule disassembly and growth via mTORC1 signaling. EMBO Rep. *22*, e51740.

Milovanovic, D., Wu, Y., Bian, X., and De Camilli, P. (2018). A liquid phase of synapsin and lipid vesicles. Science *361*, 604–607.

Molliex, A., Temirov, J., Lee, J., Coughlin, M., Kanagaraj, A.P., Kim, H.J., Mittag, T., and Taylor, J.P. (2015). Phase separation by low complexity domains promotes stress granule assembly and drives pathological fibrillization. Cell *163*, 123–133.

Moran Luengo, T., Mayer, M.P., and Rudiger, S.G.D. (2019). The hsp70-hsp90 chaperone cascade in protein folding. Trends Cell Biol. *29*, 164–177.

Murakami, T., Qamar, S., Lin, J.Q., Schierle, G.S., Rees, E., Miyashita, A., Costa, A.R., Dodd, R.B., Chan, F.T., Michel, C.H., et al. (2015). ALS/FTD mutation-induced phase transition of FUS liquid droplets and reversible hydrogels into irreversible hydrogels impairs RNP granule function. Neuron *88*, 678–690.

Murray, D.T., Kato, M., Lin, Y., Thurber, K.R., Hung, I., Mcknight, S.L., and Tycko, R. (2017). Structure of FUS protein fibrils and its relevance to self-assembly and phase separation of low-complexity domains. Cell *171*, 615–627.e16.

O'Meara, T.R., O'meara, M.J., Polvi, E.J., Pourhaghighi, M.R., Liston, S.D., Lin, Z.Y., Veri, A.O., Emili, A., Gingras, A.C., and Cowen, L.E. (2019). Global proteomic analyses define an environmentally contingent Hsp90 interactome and reveal chaperone-dependent regulation of stress granule proteins and the R2TP complex in a fungal pathogen. PLoS Biol. *17*, e3000358.

Pare, J.M., Tahbaz, N., Lopez-Orozco, J., Lapointe, P., Lasko, P., and Hobman, T.C. (2009). Hsp90 regulates the function of argonaute 2 and its recruitment to stress granules and P-bodies. Mol. Biol. Cell *20*, 3273–3284.

Patel, A., Lee, H.O., Jawerth, L., Maharana, S., Jahnel, M., Hein, M.Y., Stoynov, S., Mahamid, J., Saha, S., Franzmann, T.M., et al. (2015). A liquid-to-solid phase transition of the ALS protein FUS accelerated by disease mutation. Cell *162*, 1066–1077.

Polier, S., Dragovic, Z., Hartl, F.U., and Bracher, A. (2008). Structural basis for the cooperation of Hsp70 and Hsp110 chaperones in protein folding. Cell *133*, 1068–1079.

Qamar, S., Wang, G., Randle, S.J., Ruggeri, F.S., Varela, J.A., Lin, J.Q., Phillips, E.C., Miyashita, A., Williams, D., Strohl, F., et al. (2018). FUS phase separation is modulated by a molecular chaperone and methylation of arginine cation-pi interactions. Cell *173*, 720–734.e15.

Ramaswami, M., Taylor, J.P., and Parker, R. (2013). Altered ribostasis: RNA-protein granules in degenerative disorders. Cell *154*, 727–736.

Sanders, D.W., Kedersha, N., Lee, D.S.W., Strom, A.R., Drake, V., Riback, J.A., Bracha, D., Eeftens, J.M., Iwanicki, A., Wang, A., et al. (2020). Competing protein-RNA interaction networks control multiphase intracellular organization. Cell *181*, 306–324.e28.

Shukla, S., and Parker, R. (2016). Hypo- and hyper-assembly diseases of RNA-protein complexes. Trends Mol. Med. *22*, 615–628.

Sondermann, H., Scheufler, C., Schneider, C., Hohfeld, J., Hartl, F.U., and Moarefi, I. (2001). Structure of a Bag/Hsc70 complex: convergent functional evolution of Hsp70 nucleotide exchange factors. Science *291*, 1553–1557.

Strom, A.R., Emelyanov, A.V., Mir, M., Fyodorov, D.V., Darzacq, X., and Karpen, G.H. (2017). Phase separation drives heterochromatin domain formation. Nature *547*, 241–245.

Su, X., Ditlev, J.A., Hui, E., Xing, W., Banjade, S., Okrut, J., King, D.S., Taunton, J., Rosen, M.K., and Vale, R.D. (2016). Phase separation of signaling molecules promotes T cell receptor signal transduction. Science *352*, 595–599.

Wang, B., Maxwell, B.A., Joo, J.H., Gwon, Y., Messing, J., Mishra, A., Shaw, T.I., Ward, A.L., Quan, H., Sakurada, S.M., et al. (2019). ULK1 and ULK2 regulate stress granule disassembly through phosphorylation and activation of VCP/p97. Mol. Cell *74*, 742–757.e8.

Yang, P., Mathieu, C., Kolaitis, R.M., Zhang, P., Messing, J., Yurtsever, U., Yang, Z., Wu, J., Li, Y., Pan, Q., et al. (2020). G3BP1 is a tunable switch that triggers phase separation to assemble stress granules. Cell *181*, 325–345.e28.

Yoshizawa, T., Ali, R., Jiou, J., Fung, H.Y.J., Burke, K.A., Kim, S.J., Lin, Y., Peeples, W.B., Saltzberg, D., Soniat, M., et al. (2018). Nuclear import receptor inhibits phase separation of FUS through binding to multiple sites. Cell *173*, 693–705.e22.

Yu, H., Lu, S., Gasior, K., Singh, D., Vazquez-Sanchez, S., Tapia, O., Toprani, D., Beccari, M.S., Yates, J.R., 3rd, Da Cruz, S., et al. (2021). HSP70 chaperones RNA-free TDP-43 into anisotropic intranuclear liquid spherical shells. Science *371*, eabb4309.

Zeng, M., Chen, X., Guan, D., Xu, J., Wu, H., Tong, P., and Zhang, M. (2018). Reconstituted postsynaptic density as a molecular platform for understanding synapse formation and plasticity. Cell *174*, 1172–1187.e16.

STAR★METHODS

KEY RESOURCES TABLE

REAGENT or RESOURCE	SOURCE	IDENTIFIER
Antibodies		
G3BP1	BD	RRID:AB_398438
Hsp70	Abcam	RRID:AB_733035
Bacterial and virus strains		
BL21 (DE3) *E. coli*	TransGenBiotech	Cat#CD601-03
Chemicals, peptides, and recombinant proteins		
Hsp70	This study	N/A
Hsp70-NTD	This study	N/A
Hsp70-CTD	This study	N/A
MBP-FUS-EGFP	This study	N/A
FUS-LC	This study	N/A
Experimental models: Cell lines		
HeLa	Cell Bank of the Chinese Academy of Sciences	SCSP-504
Oligonucleotides		
UUCUCCGAACGUGUCACGUTT	Genepharma	N/A
CCAAGCAGACGCAGAUCUUTT	Genepharma	N/A
GCUGUUGUCCAGUCUGAUATT	Genepharma	N/A
Software and algorithms		
ImageJ	NIH	https://imagej.nih.gov/ij/
GraphPad Prism Software	GraphPad	https://www.graphpad.com/scientificsoftware/prism/

RESOURCE AVAILABILITY

Lead contact

Further information and requests for resources and materials should be directed to and will be fulfilled by the lead contact, Dan Li (lidan2017@sjtu.edu.cn).

Materials availability

The materials generated in this study are available from the lead contact without restriction.

Data and code availability

All data supporting the findings of this study are presented within the article and supplemental information. This paper does not report original code. All other data are available from the lead contact upon reasonable request.

METHOD DETAILS

Plasmid construction, protein expression and purification

For expression in *E. coli*, full-length Hsp70, Hsp70-NTD (residues 1–386) and Hsp70-CTD (residues 387–641) were cloned into vector pET28a with an N-terminal His_6 tag. Full-length FUS was cloned into pET32a vector containing an MBP-His_6 tag fused at the N terminus and an EGFP tag at the C terminus. FUS-LC (residues 1–163) was cloned into pET22b vectors with an N-terminal His_6 tag. For expression in mammalian cell lines, RFP-FUS R521H were subcloned into pCAG vector.

For protein purification, full-length Hsp70 and its domains (Hsp70-NTD and Hsp70-CTD) were induced to express in *E. coli* BL21 (DE3) after adding 1 mM IPTG. After induction, cells grew at 16°C for 16 h, then the cells were lysed in 50 mM Tris-HCl (pH 7.5), 500 mM NaCl, 4 mM β-mercaptoethanol, 2 mM PMSF. Cell supernatant was collected after centrifugation (14,000 rpm, 4°C, 30 min) and subjected to Ni column (GE Healthcare). Proteins were then eluted by elution buffer containing 50 mM Tris-HCl (pH 7.5), 100 mM NaCl, and 150 mM imidazole. The eluted proteins were concentrated and subjected to size-exclusion chromatography column Superdex 75 16/60 (GE Healthcare) in 50 mM Tris-HCl (pH 7.5), 100 mM NaCl and 2 mM DTT. All proteins were concentrated and then quickly frozen in liquid nitrogen. The cleavage of his-tag was performed by bivine Thrombin (Yeasen), and the purity of Hsp70 was confirmed by SDS-PAGE and western blot. We measured the 260/280 ratio of the purified protein by Nanodrop 2000 (ThermoFisher) to be 0.58, indicating that the purified protein was free of nucleic acid contamination.

Full-length MBP-FUS-EGFP was expressed in *E. coli* BL21 (DE3) cells. Cells were grown to an OD_{600} of 0.8 and then incubated with 0.5 mM IPTG overnight at 16°C. Cells were lysed with the lysis buffer containing 50 mM Tris-HCl (pH 8.0), 500 mM NaCl, 10 mM imidazole, 4 mM β-mercaptoethanol, and 100 μg ml^{-1} RNase A, and 1 mM PMSF. Then the cell supernatant was collected and loaded onto Ni column (GE Healthcare). The protein was eluted with 50 mM Tris-HCl (pH 8.0), 500 mM NaCl, 100 mM imidazole, and 4 mM β-mercaptoethanol. Then the MBP-His_6 tag was cleaved by GST-tagged 3C prescission protease during dialysis in 50 mM Tris-HCl (pH 7.4), 1 M KCl, 10% glycerol, 4 mM β-mercaptoethanol for 4 h. The cleaved MBP-His and 3C protease were further removed with Ni column and Glutathione Sepharose column (GE Healthcare). Then the protein was concentrated and subjected into size-exclusion chromatography column Superdex 200 16/600 in 50 mM Tris-HCl (pH 7.5), 500 mM KCl, 2 mM DTT and 10% glycerol.

FUS-LC (residues 1–163) was expressed in *E. coli* BL21 (DE3) and then induced with 0.5 mM IPTG at 16°C for 48 h. Cells were collected and lysed by sonication in 50 mM Tris-HCl (pH 8.0), 6 M guanidine hydrochloride on the ice. Cell pellet was removed by centrifugation (14,000 rpm, 4°C, 40 min) and then cell supernatant was loaded onto a Ni column after filtration. Protein was eluted in 50 mM Tris-HCl (pH 8.0), 6 M guanidine hydrochloride and 50 mM imidazole. Further the eluted protein was purified via high performance liquid chromatography (HPLC) (Agilent) and freeze dried by FreeZone lyophilizer (Thermo Fisher). FUS-LC powder was dissolved into 50 mM Tris-HCl (pH 8.0), 8 M urea and then desalted into 5 mM CAPS (pH 11.0) for long-term storage. For further experiments, the concentrated FUS-LC was diluted into each individual buffer solution to aimed concentration.

Fluorescent labeling of proteins

For labeling proteins with active amine groups, Hsp70 was desalted into reaction buffer containing 50 mM NaPhosphate (pH 7.0), 50 mM NaCl. The proteins were then incubated with a 5-fold Alexa 488 C_5-malemide (Invitrogen, A10254) for 1 hour at room temperature. Then, the labeled proteins were further purified with a Superdex 75 10/300 size-exclusion chromatography column (GE Healthcare) in 50 mM NaPhosphate (pH 7.0), 50 mM NaCl. Hsp70-NTD and Hsp70-CTD performed the same labeling procedure as that for full-length Hsp70. For Hsp70 with active thiol groups, Hsp70 was desalted into reaction buffer containing 50 mM Tris-HCl (pH 7.5), 100 mM NaCl and 4 mM Tris (2-Carboxyethyl) Phosphine (TCEP) (Invitrogen, T2556) to remove DTT in storage buffer and then incubated with a 5-fold Alexa 647 C_2-malemide (Invitrogen, A20347) for 1 hour at room temperature. The labeled protein was subjected to size-exclusion chromatography column Superdex 75 10/300 in 50 mM PBS (pH 7.0), 500 mM NaCl. For further LLPS experiments and confocal imaging, the unlabeled protein was mixed with the fluorescent labeled protein with the molar ratio of 50:1 (unlabeled: labeled).

In vitro LLPS assay

For the protein LLPS assay, all experiments were performed at room temperature. 50 μM full-length Hsp70 and its domains phase separated in the buffer containing 50 mM Tris-HCl (pH 7.5), 100 mM NaCl and PEG 3,350 (0–10%). The LLPS of FUS-EGFP was induced in the buffer containing 50 mM Tris-HCl (pH 7.5), 100 mM NaCl. For co-LLPS experiments, 10/2 μM FUS-EGFP were mixed with 1/0.2/50 μM Hsp70 in the buffer containing 50 mM Tris-HCl (pH 7.5), 100 mM NaCl; 10/2 μM EGFP were mixed with 1/0.2 μM Hsp70 in the buffer containing 50 mM Tris-HCl (pH 7.5), 100 mM NaCl; or, 50/5 μM Hsp70 were mixed with 2/0.2 μM FUS-EGFP/EGFP in the buffer containing 50 mM Tris-HCl (pH 7.5), 100 mM NaCl and 10% PEG 3,350.

Differential interference contrast (DIC) and fluorescent imaging for protein LLPS

LLPS samples were loaded onto glass slides and sealed with coverslip. DIC images of LLPS and co-LLPS samples were acquired on a Leica TCS SP8 microscope with a 100× objective (oil immersion) at room temperature. Fluorescent images of protein samples were acquired with the Leica TCS SP8 confocal microscopy using a 100× objective (oil immersion) at a resolution 2,048× 2,048 pixel.

Turbidity measurement

LLPS of Hsp70 and its domains were induced in the buffer as described above. Turbidity measurements were conducted at 600 nm in a 384-well plate with 20 μL samples using a Varioskan Flash spectral scanning multimode reader (Thermo Fisher).

Fluorescence recovery after photobleaching (FRAP)

All FRAP experiments were performed on a Leica TCS SP8 microscope with 100× oil objective by using the FRAP module. For protein samples, 20 μL LLPS sample of Hsp70 or its domains was placed in a glass bottom dish (Nest, 80100). FRAP images were acquired at 488 nm and performed with 1,024 × 1,024 pixel. Bleaching area of droplet was restricted to a graphical region and then quenched for 2.58 s at full laser power. After photo bleaching, images were obtained at 2.58 s/frame.

For living cells assay, HeLa cells were grown in chambered coverglass (Thermo Fisher Scientific, 155,383), and then transfected with mEGFP-G3BP1 or RFP-FUS R521H. Cells were treated with 100 μM of sodium arsenite for indicated time to induce SGs after culturing for 24 h. SGs were bleached by a 488 nm or 561 nm laser at 100% power and then acquired time-lapse images at 2.58 s per frame for indicated time. Data analysis were processed by Fiji and GraphPad Prism. All experiments were repeated independently for more than three times. All statistic values were displayed as mean ± S.D. The statistical significance in this study is determined by the unpaired, two-tailed Student's *t* test. $p > 0.05$ is set to not significant; *$p < 0.05$; **$p < 0.01$.

Nuclear magnetic resonance (NMR)

All titration experiments were performed at 298 K or 288 K on a Bruker 900 MHz spectrometer equipped with cryogenically cooled probes. The his-tag of Hsp70 was cleaved by thrombin. The labeled protein of ^{15}N-FUS-LC was prepared in the NMR buffer (25 mM MES, 100 mM NaCl, and 10% D_2O) at different pH (pH 6.1/6.6). Before experiments, full-length Hsp70 and its domains were desalted into the indicated NMR buffer. Each NMR sample was prepared to a volume of 500 μL containing ^{15}N-FUS-LC (25 μM) and indicated concentrations of Hsp70 or its domains. The ^{15}N increments of the NMR samples were increased to 256. The backbone assignment of FUS-LC was accomplished based on previous studies (Burke et al., 2015), and all NMR data were processed by NMRpipe and analyzed by SPARK (Delaglio et al., 1995; Lee et al., 2015).

Thioflavin T (ThT) fluorescence assay

All ThT experiments were performed in ThT assay buffer containing 50 mM Tris-HCl (pH 7.5), 100 mM NaCl, 50 μM ThT and 0.05% NaN_3 was incubated with 0.5% preformed FUS-LC fibril seeds (monomer equivalence) in 384-well plates (Corning) at 25°C. Each ThT sample was prepared to a volume of 60 μL containing FUS-LC (25 μM) and indicated concentrations of Hsp70 or its domains. The Varioskan Flash spectral scanning multimode reader (Thermo Fisher Scientific) was used to monitor the ThT fluorescence with excitation at 440 nm and emission at 485 nm. The sample plate was shaken at 600 rpm for 10 seconds before each measurement of ThT fluorescent intensity.

Cell cultures and transfection

HeLa cells (Cell Bank of the Chinese Academy of Sciences, Shanghai, SCSP-504) were cultured in the Dulbecco's Modified Eagle Medium (sigma, D0819) supplemented with 10% (v/v) fetal bovine serum (FBS, BioWest) and 1% penicillin/streptomycin at 37°C in 5% CO_2. According to the manufacturer's instruction, PolyJet™ reagent (SignaGen, SL100688) was used for the transfection of plasmids into HeLa cells, follow-up experiments were performed 24 h after cell transfection. In the knockdown assay, the siRNA (Genepharma) was transfected into the HeLa cells using the LipofectamineTM RNAiMax Transfection Reagent (Invitrogen) according to the manufacturer's instruction. Cells were harvested after incubation with siRNA for 48–72 h. The siRNA oligos used in this study are listed below:

si-Ctrl: 5'- UUCUCCGAACGUGUCACGUTT -3';

si-Hsp70: 5′- CCAAGCAGACGCAGAUCUUTT -3′;

si-Hsc70: 5′- GCUGUUGUCCAGUCUGAUATT -3′

Induction of stress granules by arsenite stress

HeLa cells were grown on coverslips in a 24-well plate or grown in chambered coverglass (Thermo Fisher Scientific, 155383), and then transfected with the indicated plasmids or siRNA. Cells were then treated with 100 μM $NaAsO_2$ for indicated time.

Immunostaining and confocal imaging

HeLa cells were grown on coverslips in the 24-well plate before transcription and treatment. The cells were then fixed in 4% paraformaldehyde in PBS for 15 min at room temperature, permeabilized in 0.5% TritonX-100 (Sigma) in PBS for 15 min and blocked with 3% goat serum in PBST (PBS + 0.1% Triton X-100) for 1 h. Cells were incubated with anti-G3BP1 antibody (BD, 611127) and anti-Hsp70 antibody (Abcam, ab45133) overnight at 4°C or at room temperature for 1–2 h. AlexaFluor-488 (Invitrogen, A11001) and AlexaFluor-647 (Invitrogen, A11011) were used as the second antibodies, respectively. After washing for 3 times with PBST, cells were mounted on glass slides using the ProLong™ Gold Antifade Mountant with DAPI (ThermoFisher, P36935). Fluorescent images were taken using the Leica TCS SP8 confocal microscopy system using 100× oil objective. Images were processed and assembled into figures using LAS X (Leica) and Fiji.

QUANTIFICATION AND STATISTICAL ANALYSIS

GraphPad Prism and Microsoft Excel software were used for statistical analysis. All experiments were repeated independently for more than three times. All statistic values were displayed as mean ± S.D. The statistical significance in this study is determined by the unpaired, two-tailed Student's *t* test, $p > 0.05$ is set to not significant, $^*p < 0.05$, $^{**}p < 0.01$.